

Neural Diffusion Processes for Physically Interpretable Survival Prediction

Alessio Cristofolletto*

Department of Computing Sciences, Bocconi University, Milano, Italy

Cesare Rollo,* Giovanni Birolo, and Piero Fariselli

AI and Computational Biomedicine Unit, University of Torino, Torino, Italy

(Dated: October 3, 2025)

We introduce *DeepFHT*, a survival-analysis framework that couples deep neural networks with first hitting time (FHT) distributions from stochastic process theory. Time to event is represented as the first passage of a latent diffusion process to an absorbing boundary. A neural network maps input variables to physically meaningful parameters including initial condition, drift, and diffusion, within a chosen FHT process such as Brownian motion, both with drift and driftless. This yields closed-form survival and hazard functions and captures time-varying risk without assuming proportional-hazards.

We compare DeepFHT with Cox survival model using synthetic and real-world datasets. The method achieves predictive accuracy on par with state-of-the-art approaches, while maintaining a physics-based interpretable parameterization that elucidates the relation between input features and risk. This combination of stochastic process theory and deep learning provides a principled avenue for modeling survival phenomena in complex systems.

I. INTRODUCTION

Survival analysis is central in many applications across medicine, engineering, economics and finance. It concerns *time-to-event modeling*: given a process that can generate an event of interest (e.g., death from disease, failure due to wear), the goal is to estimate the probability that an event occurs at time t for an individual described by input variables (or features, or covariates). Unlike standard regression settings, survival data are characterized by censoring, which means that for some instances, the exact event time is not observed (for example, when they remain event-free at the end of the study), and only the last recorded follow-up time is available.

Traditional approaches to survival modeling rely on strong statistical assumptions linking input variables and risk. The Cox proportional hazards (CoxPH) model [1] remains the most widely used and best established method. The proportional hazards assumption implies that the instantaneous risk of an event for two individuals differs by a constant factor over time. The Cox model is also linear, making it clear how each single input variable affects the outcome, but at the expense of missing interactions between features. In its original form, this relation is modeled through a linear regression on the features, though many extensions have been developed to relax linearity and improve performance in high-dimensional settings [2–4].

Despite its success, Cox regression is limited by the proportional hazards (PH) assumption, which is often unrealistic. Consequently, many alternatives have been proposed that dispense with the PH constraint, ranging from classical statistical formulations [5, 6] to mod-

ern methods that incorporate machine learning and deep learning techniques [7–9].

Among these, *first hitting time* (FHT) models are of particular interest for this work. FHT models assume that event times are distributed as the times of first passage of a latent stochastic process, underlying the event-generating process observed, through a barrier. This approach overcomes the PH assumption, since FHT distributions for many stochastic processes allow for time-varying hazard ratios between different individuals (e.g., Lévy distribution, inverse Gaussian distribution).

A branch of FHT methods aims to model the distribution of first hitting times directly, using machine learning techniques [10] and deep neural networks [11] to achieve strong predictive performance, but often failing to give interpretable insights into the nature of the underlying process and how features relate to it, due to the black box nature of most deep learning frameworks. Conversely, parametric FHT alternatives [12–14] currently suffer from the opposite drawbacks. These models learn the process parameters on which the distribution of first hitting times depends from data, using simpler regression and machine learning techniques, yielding more physically interpretable results at the expense of model expressiveness.

The present work proposes a framework that combines these complementary strengths. Our model, *DeepFHT*, integrates parametric FHT modeling with deep neural networks, which are used to map input features to the parameters of the underlying stochastic process. To our knowledge, this is the first application of modern deep learning techniques to parametric FHT models for survival prediction. The hybrid design leverages the representational capacity of neural networks while preserving interpretability through the physical meaning of process parameters. In this way, DeepFHT offers a controlled alternative to black-box survival models: while it does

* These authors contributed equally to this work.

not eliminate the challenges of interpretability, it grounds predictions in a dynamical description that connects input features to the evolution of an underlying stochastic process.

We demonstrate the capability of our framework on synthetic and publicly available clinical survival datasets, comparing performance against the Cox model. DeepFHT achieves competitive accuracy across clinical benchmarks and clearly outperforms Cox regression on synthetic data designed to probe the model’s capabilities in scenarios with nonlinearities and non-proportional hazards. Finally, we assess interpretability by examining correlations between predicted process parameters, empirical risk and features. The results show that similarity between patient outcomes is intuitively encoded as distance in the space of parameters, and that DeepFHT can recover clinically meaningful relationships and has the potential to highlight new correlations in complex, high-dimensional data.

The remainder of the paper is organized as follows. In Section II and Section III we briefly present the central problem of survival analysis and the necessary theory of stochastic processes. Section IV presents the proposed model and the experimental setup, while results and the notion of *physics-based interpretability* of the model are discussed in Section V.

II. SURVIVAL ANALYSIS FRAMEWORK

Survival data are typically represented as triplets $(\mathbf{x}_i, \delta_i, T_i)$ for $i = 1, \dots, n$, where:

- $\mathbf{x}_i \in \mathbb{R}^m$ is a vector of features
- $\delta_i \in \{0, 1\}$ is an indicator that denotes whether the event was observed ($\delta_i = 1$) or the instance was right censored, i.e., end of observation without occurrence of the event ($\delta_i = 0$)
- T_i is the time of event occurrence or censoring
- n is the dataset size

The goal of survival analysis is to predict the probability distribution of event times $f(t)$ and some relevant, related quantities:

- survival function $S(t) = \Pr(T > t)$
- cumulative distribution function $F(t) = 1 - S(t)$
- hazard function

$$h(t) = \lim_{\Delta t \rightarrow 0^+} \frac{\Pr(t \leq T < t + \Delta t \mid T \geq t)}{\Delta t} = \frac{f(t)}{S(t)},$$

The survival function describes the probability of surviving beyond time t , while the hazard captures the instantaneous risk of event occurrence given survival up to t . Estimation typically focuses on conditional forms $S(t|\mathbf{X})$ and $h(t|\mathbf{X})$, which quantify the dependence of survival dynamics on features.

III. FIRST HITTING TIME MODELS FOR SURVIVAL ANALYSIS

A natural probabilistic representation of survival processes is provided by the theory of first hitting times. Consider a 1D continuous-time stochastic process $\{X(t)\}_{t \geq 0}$, with $X(t) \in \mathbb{R}$, described by a probability distribution $p(x, t)$. Let $\Gamma : \{x \leq x_b\} \subset \mathbb{R}$ be a target set and $X(t = 0) = x_0 > x_b$ the initial condition. In this setup, x_b can be considered as a barrier between the target set and the initial condition and this is how it will be referred to in the rest of the paper. The first hitting time is then

$$T = \inf\{t > 0 : X(t) \in \Gamma\}, \quad (1)$$

that is, the earliest time at which the process crosses the barrier in x_b . When the barrier is considered to be absorbing (i.e., killing the process upon transition), the distribution $f(T)$ of first hitting times coincides with the event time distribution in survival analysis. This condition is easily imposed by the Dirichlet condition $p(x_b, t \mid x_0) = 0$. Without losing generalizability, we will always consider positive initial conditions $x_0 > 0$ and an absorbing barrier in $x_b = 0$. This amounts to a generic choice for a process in $X(t) \in \mathbb{R}$.

Since all relevant survival functions can be derived from the distribution of first hitting times $f(T)$, it is crucial to have analytical solutions for this quantity. In this work, we consider two stochastic processes whose theory is well developed and for which an analytical solution is available: the *Brownian motion* and the *arithmetic Brownian motion* (Brownian motion with drift). For a more complete and detailed discussion of FHT theory and models, including but not limited to their application to survival analysis, we refer to [12, 15, 16].

A. First hitting time and survival distributions for Brownian motion

Brownian motion is a pure diffusion process described by a probability distribution $p(x, t \mid x_0)$ that evolves according to the Fokker–Planck equation:

$$\frac{\partial}{\partial t} p(x, t \mid x_0) = D \frac{\partial^2}{\partial x^2} p(x, t \mid x_0), \quad (2)$$

with constant diffusion coefficient $D > 0$ and initial condition $p(x, 0 \mid x_0) = \delta(x - x_0)$. Imposing an absorbing barrier at $x_b = 0$ corresponds to the Dirichlet boundary condition

$$p(0, t \mid x_0) = 0, \quad x_0 > 0.$$

The method of images yields the transition probability density (exact solution):

$$p(x, t \mid x_0) = \frac{1}{\sqrt{4\pi Dt}} \left[\exp\left(-\frac{(x - x_0)^2}{4Dt}\right) - \exp\left(-\frac{(x + x_0)^2}{4Dt}\right) \right] \quad (3)$$

This solution describes a Brownian motion starting at $x_0 > 0$ with an absorbing barrier at the origin.

From the probability distribution (3), all relevant survival quantities can be derived. We focus specifically on:

- **Survival function**

$$S(t) = \int_0^\infty p(x, t | x_0) dx = \operatorname{erf}\left(\frac{x_0}{\sqrt{4Dt}}\right), \quad (4)$$

- **Failure density**

$$f(t) = -\frac{d}{dt}S(t) = \frac{x_0}{2\sqrt{\pi}} \frac{\exp(-x_0^2/(4Dt))}{(Dt)^{3/2}}, \quad (5)$$

the distribution of first hitting times (i.e., event times)

The Brownian FHT model is characterized by a failure density that has the form of a Lévy distribution, depending only on process parameters x_0, D .

B. First hitting time and survival distributions for arithmetic Brownian motion

Adding a constant drift term μ to Brownian motion yields the *arithmetic Brownian motion*. For this process, the Fokker-Planck equation becomes:

$$\frac{\partial}{\partial t}p(x, t | x_0) = -\mu \frac{\partial}{\partial x}p(x, t | x_0) + D \frac{\partial^2}{\partial x^2}p(x, t | x_0), \quad (6)$$

with constant diffusion coefficient $D > 0$. For an initial condition $p(x, 0 | x_0) = \delta(x - x_0)$, the solution is Gaussian with the mean shifted linearly in time:

$$p(x, t | x_0) = \frac{1}{\sqrt{4\pi Dt}} \exp\left(-\frac{(x - x_0 - \mu t)^2}{4Dt}\right). \quad (7)$$

Introducing an absorbing barrier at $x_b = 0$ modifies the solution which becomes, via the method of images:

$$p(x, t | x_0) = \frac{1}{\sqrt{4\pi Dt}} \left[\exp\left(-\frac{(x - x_0 - \mu t)^2}{4Dt}\right) - \exp\left(-\frac{\mu x_0}{D}\right) \exp\left(-\frac{(x + x_0 - \mu t)^2}{4Dt}\right) \right], \quad (8)$$

valid for $x > 0, x_0 > 0$.

From (8), the survival analysis quantities follow:

- **Survival function**

$$\begin{aligned} S(t) &= \Pr(T > t) \\ &= \Phi\left(\frac{x_0 + \mu t}{\sqrt{2Dt}}\right) - \exp\left(-\frac{\mu x_0}{D}\right) \Phi\left(\frac{\mu t - x_0}{\sqrt{2Dt}}\right), \end{aligned} \quad (9)$$

where $\Phi(\cdot)$ denotes the standard normal cdf

- **Failure density**

$$f(t) = \frac{x_0}{\sqrt{4\pi Dt^3}} \exp\left(-\frac{(x_0 + \mu t)^2}{4Dt}\right), \quad (10)$$

which corresponds to an inverse Gaussian distribution

In the limit $\mu \rightarrow 0$, these expressions reduce to the driftless Brownian case, with the failure density converging to the Lévy distribution. Given sufficient time, failure is certain only for $\mu < 0$.

IV. METHODS

A. DeepFHT

As outlined in Sec. III, survival outcomes can be modeled by first hitting time (FHT) distributions with absorbing barriers. The corresponding survival functions and event-time distributions are determined by the choice of underlying process, depending explicitly on its parameters.

To model these functions and distributions from data, we employ a feedforward neural network f_θ that maps features $\mathbf{x}_i \in \mathbb{R}^m$ to a vector of distributional parameters $\mathbf{p}_i = f_\theta(\mathbf{x}_i) \in \mathbb{R}^d$, i.e. the parameters of the underlying stochastic process. The parameterizations \mathbf{p}_i produced by the network are then used to evaluate survival quantities such as $S(t | \mathbf{x}_i) = S(t; \mathbf{p}_i)$, $F(t | \mathbf{x}_i) = F(t; \mathbf{p}_i)$, where S and F denote the functional forms of the survival and failure distributions of the chosen FHT model.

The dimension d of the output vector \mathbf{p} depends on the choice of parametrization of the FHT distribution. As anticipated in Section III, in this paper we will focus on Brownian and arithmetic Brownian motion, identified by their FHT distributions 5,10, with the following parameterizations:

- **Lévy distribution:** $\mathbf{p} = (x_0, D)_\theta$,
- **Inverse Gaussian distribution:** $\mathbf{p} = (x_0, \mu)_\theta$ with $\mu < 0, D = 1$,

For the inverse-Gaussian model we fix $D = 1$ without loss of generality. The FHT law depends on $\mu_T = x_0/|\mu|$ and $\lambda = x_0^2/(2D)$, thus D only sets the time scale and can be absorbed by rescaling time (or μ). We therefore parameterize the model by (x_0, μ) with $\mu < 0$.

Notably, both parameterizations above allow for non-proportional hazards, reflecting the flexibility of FHT-based models to capture complex time dependencies in risk. Figure 1 illustrates a representative model output, where survival functions are computed from the estimated distributional parameters for a set of individuals.

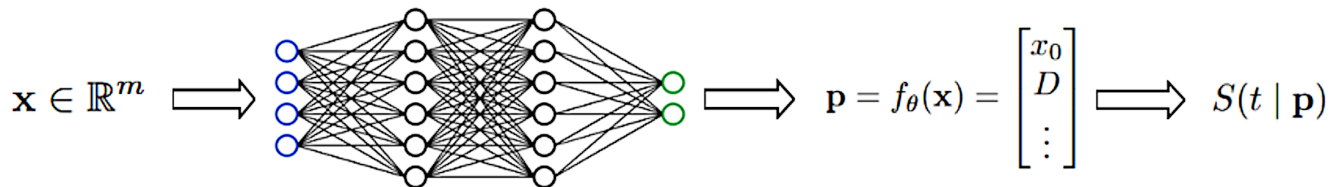


FIG. 1: Example output of the Lévy FHT model. Individual-specific survival functions are computed from the neural network-predicted parameters.

It is also worth noting that this model can easily be extended to any other probability distribution of choice. It is sufficient to specify the functional form and its parameterization and to modify the size of the output layer accordingly. In Sec. IV C we take advantage of this flexibility to compare results obtained with Lévy and Inverse Gaussian distributions against those obtained with failure density distributions that have no direct interpretation in the first hitting time framework.

B. Loss function: Brier loss

Training is performed by minimizing a custom *Brier loss*, adapted from the Brier score [17, 18] (see Sec. IV C) commonly used to evaluate probabilistic forecasts. For a given set of unique observed event times $T = \{T_j : \delta_j = 1\}$, the loss is defined as

$$\mathcal{L} = \sum_{t \in T} \sum_i \left[I(T_i \leq t \wedge \delta_i = 1) (S(t|\mathbf{x}_i))^2 + I(T_i > t) (1 - S(t|\mathbf{x}_i))^2 \right], \quad (11)$$

where $S(t|\mathbf{x}_i)$ denotes the survival probability predicted for subject i , and $I(\cdot)$ is the indicator function.

C. Experimental setup

The experimental evaluation of DeepFHT tests model performance when modeling first hitting time distributions for diffusion processes (Lévy, inverse Gaussian). As an external benchmark, we also include the Cox proportional hazards model, the standard reference in survival analysis.

The procedure consists of two phases. First, for each candidate distribution, we perform 5-fold cross-validation on a training set comprising 80% of the available data, with the remaining 20% held out for testing. Each split preserves the original ratio of observed to censored instances. Cross-validation is used to select the optimal architecture and hyperparameters (see Appendix A), based on average validation performance measured over 100 trials. For hyperparameter search, we use the *Optuna* framework [19], which implements efficient strategies for exploring the hyperparameter space.

After hyperparameter optimization, models are re-trained on the full training set and evaluated on the held-out test set. For each performance metric, mean and standard deviation are estimated via bootstrap resampling: 100 datasets of equal size are drawn with replacement from the test set, each preserving the censoring ratio.

Performance metrics

Antolini's C-index. We use the time-dependent concordance index (also referred to as *Antolini's C-index*) [20] as the performance metric of choice, for both validation and testing. It is a rank statistic that measures agreement between predicted risks and observed survival times as the probability that, among two comparable individuals, the one experiencing the event earlier is assigned a higher predicted risk (or equivalently a lower survival probability). While time-independent in its original formulation [21], Antolini's formulation generalizes the measure to time-dependent predictions:

$$c = \frac{\sum_{(i,j)} w(T_i) I(T_i < T_j \wedge \delta_i = 1 \wedge S(T_i | \mathbf{X}_i) < S(T_i | \mathbf{X}_j))}{\sum_{(i,j)} w(T_i) I(T_i < T_j \wedge \delta_i = 1)} \quad (12)$$

where $w(T_i)$ are inverse probability of censoring weights (IPCW) [22], used to correct for bias introduced by censoring. This time-dependent version is equivalent to the ROC-AUC and is more appropriate for evaluating models whose predictions vary with time.

Integrated Brier score. The Brier score [17] measures predictive accuracy as the mean squared difference between predicted survival probabilities and observed outcomes δ_i . Its time-dependent extension [18] evaluates survival probabilities $S(t | \mathbf{X}_i)$ at arbitrary times t and uses IPCW. This yields a curve $B(t)$ describing calibration and discrimination across time. To summarize performance over the full observation window, we report the integrated Brier score (IBS),

$$B = \frac{1}{t_{\max} - t_0} \int_{t_0}^{t_{\max}} B(t) dt, \quad (13)$$

where lower values indicate better overall predictive accuracy. In our experiments, the IBS is used as an additional metric during the testing phase only.

Datasets

We evaluate DeepFHT on publicly available clinical survival datasets, accessed through the *SurvSet* [23] repository, as well as on a synthetic dataset designed to test non-proportional hazards and nonlinear relationships between features and risk.

All datasets undergo identical preprocessing: categorical features are one-hot encoded; missing values are imputed using the mean or median for numerical variables (depending on skewness) and the mode for categorical variables; finally, all features are scaled.

GBSG2: Data from the German Breast Cancer Study Group 2 [24], comprising 686 patients with node-positive primary breast cancer. Eight clinical features are available, with 56% censoring.

Framingham: Derived from the Framingham Heart Study [25], including 4 699 participants and 7 cardiovascular health features.

SUPPORT2: A multi-center observational study of seriously ill hospitalized adults in the United States [26]. The *SurvSet* version contains 9 105 records with 35 features; censoring accounts for 32%.

FLChain: Data from the Mayo Clinic study of free light chain (FLC) testing [27], including 7 874 patients and 10 features; 72% of cases are censored.

NonPH: A synthetic dataset introduced in [28], specifically designed to violate proportional hazards and enforce nonlinear feature-hazard relationships. It contains 10 000 individuals with 20 normally distributed features. Event times are generated by partitioning the observation period into 16 intervals and assigning individual-specific failure densities:

$$p_i = \frac{\exp(16x_i)}{\sum_{j=1}^{16} \exp(16x_j)},$$

where x_i are features. This construction yields non-proportional hazards by design (see Appendix C for more details).

V. RESULTS

A. Model performance

Test results are summarized in Figs. 2- 3. Across datasets and distributions, DeepFHT demonstrates competitive performance, consistently matching or surpassing Cox regression in terms of Antolini’s C-index. Models based on the more physically interpretable Lévy and inverse Gaussian distributions achieve the highest scores on three of the four real-world datasets, while also exhibiting strong robustness and stability at test time.

On the synthetic *NonPH* dataset, DeepFHT significantly outperforms Cox regression with all tested distri-

butions, underscoring the gains achievable in scenarios with nonlinear effects and violations of the proportional hazards assumption.

Within the clinical datasets, the comparable performance of DeepFHT and Cox regression on GBSG2, Framingham, and FLChain suggests that in these cases the assumptions of linearity and proportional hazards may not be restrictive. This points instead to potential limitations in the expressiveness or complexity of the datasets themselves. By contrast, on the higher-dimensional SUPPORT2 dataset, the inverse Gaussian variant achieves a clear improvement over Cox regression, illustrating the advantage of relaxing linear and proportional hazards assumptions in more complex clinical settings.

B. Physics-based interpretability

The parametric nature of DeepFHT, grounded in stochastic process theory, provides a natural and physically meaningful basis for interpreting its predictions. As presented in Section IV A, for each individual, the model outputs a vector of parameters of the learned underlying diffusion process, effectively representing the subject as a point in a latent parameter space. This space is inherently interpretable: because the influence of each parameter on the process dynamics is known, we are able to distinguish regions of higher or lower risk and to qualitatively compare the trajectories of individuals in this space. Crucially, such analysis can be performed without explicitly computing survival probabilities.

In our case, the parameterization of Lévy (5) and inverse Gaussian (10) distributions with DeepFHT yields a two-dimensional parameter space. This representation makes interpretation visually intuitive and, in particular, enables the use of Euclidean distance to assess similarity between instances, i.e., whether they exhibit comparable dynamics and event-time probabilities. We show this by visualizing empirical event-time distributions in the parameter space via color gradients and observing that the model consistently assigns previously unseen instances (test set data points) to regions populated by individuals with similar observed event times.

Event times in parameter space. In the parameter spaces of the Lévy and inverse Gaussian models, we visualize the risk associated with each point by interpolating event times from the training data. Only uncensored instances $\mathbf{p}_i \in U = \{\mathbf{p}_i \mid \delta_i = 1\}$ are considered, and interpolation is performed by inverse distance weighting:

$$T(\mathbf{p}) = \frac{\sum_{\mathbf{p}_i \in U} w_i(\mathbf{p}) T_i}{\sum_{\mathbf{p}_i \in U} w_i(\mathbf{p})}, \quad w_i(\mathbf{p}) = \frac{1}{\sqrt{d(\mathbf{p}, \mathbf{p}_i)}},$$

which assigns to each point \mathbf{p} in the parameter space an estimated event time $T(\mathbf{p})$. These values serve as proxies for patients’ risk and allow us to test whether the

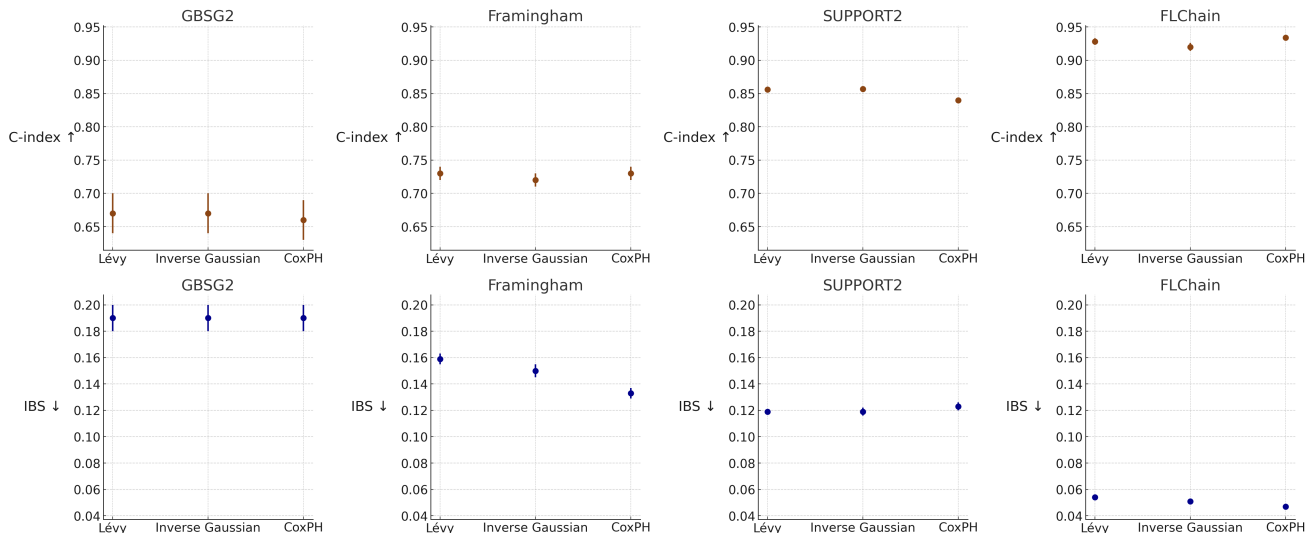


FIG. 2: Performance across clinical datasets. Scatterplots with error bars for C-index (\uparrow , brown, top row) and IBS (\downarrow , dark blue, bottom row) across four datasets (GBSG2, Framingham, SUPPORT2, FLChain). For each dataset, three models are shown: Lévy, inverse Gaussian, and CoxPH. Mean values and standard deviations are computed via 100 bootstrap iterations.

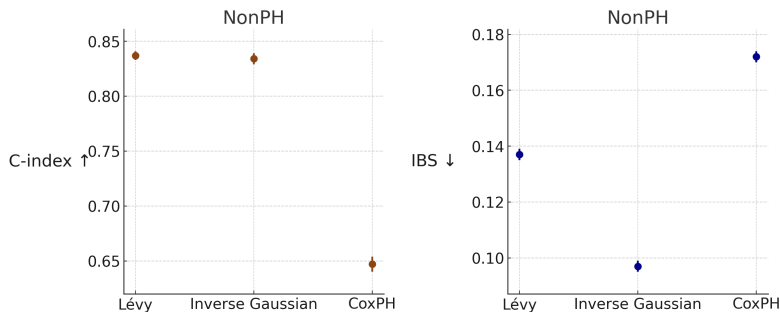


FIG. 3: Performance on the NonPH dataset. Scatterplots with error bars showing C-index (\uparrow , brown) and IBS (\downarrow , dark blue) for three models (Lévy, inverse Gaussian, CoxPH). Mean values and standard deviations are computed via 100 bootstrap iterations.

model implements a similarity notion based on distance in parameter space.

In Fig. 4, a colormap based on $T(\mathbf{p})$ is superimposed on the parameter space, with uncensored test instances and individuals surviving beyond the last uncensored time represented as points colored by their observed event times. The plots show that previously unseen patients are typically assigned to regions with comparable event times, indicating that individuals with similar risk cluster together in the space of process parameters.

We also note that the empirical distribution of event times shown in Fig. 4 — and used as a proxy for patient risk — matches our theoretical knowledge of process dynamics. Patients with longer survival times cluster in regions with favorable initial conditions (i.e., larger distance from the absorbing barrier) and lower diffusion coefficient or drift; processes with these parameter values typically yield longer first-passage times. Conversely, patients experiencing early failure are assigned higher D or μ and initial conditions closer to the barrier, consistent

with shorter first-passage times.

Feature values distribution. We further illustrate physics-based interpretability by examining the relationship between clinical features and the learned distribution parameters. For instance, in the inverse Gaussian model applied to the GBSG2 dataset, patients from the test set are mapped into the parameter space $\{x_0, \mu\}$ and tumor grade is visualized by color gradient (Fig. 5, bottom row). A clear pattern emerges: patients with low-grade tumors (grade 1) occupy regions with favorable initial conditions and weaker drift (low-risk), while those with high-grade tumors (grade 3) cluster near the absorbing barrier with stronger drift (high-risk). This distribution is consistent with established clinical understanding of tumor aggressiveness and prognosis.

A similar analysis for the Lévy model on the Framingham dataset reveals that individuals with higher systolic blood pressure (sbp) and diastolic blood pressure (dbp) are more frequently located in the high-risk region of the

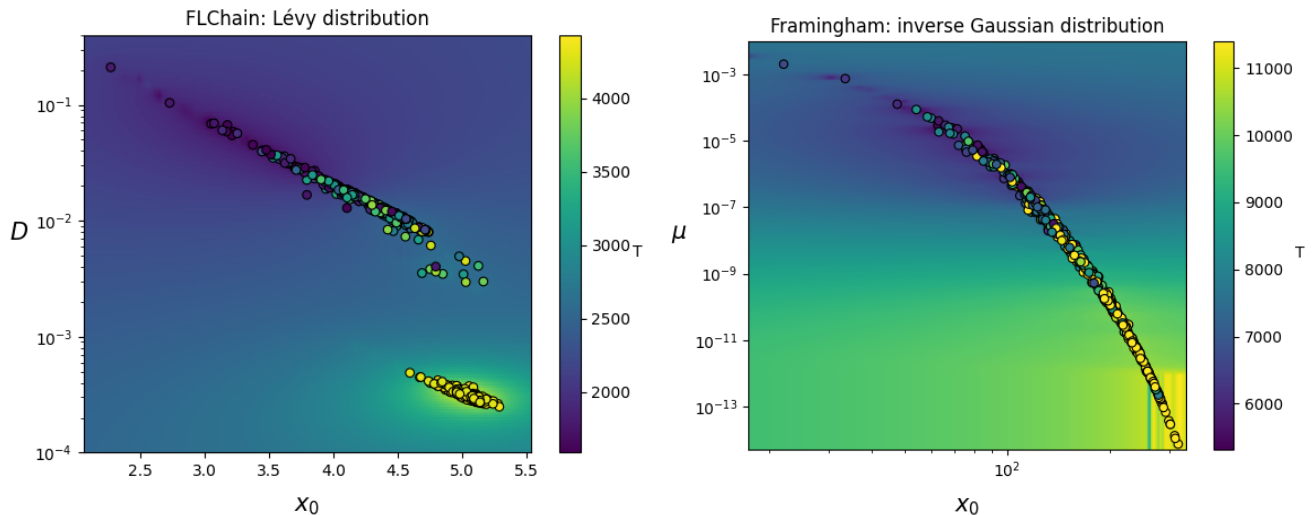


FIG. 4: Event times in the parameter spaces of Deep FHT models. Left: FLChain dataset in the space of Lévy Deep FHT ($\{x_0, D\}$). Right: Framingham dataset in the space of inverse Gaussian Deep FHT ($\{x_0, \mu\}$). Background colors represent interpolated event times $T(\mathbf{p})$ obtained by inverse distance weighting of uncensored training instances. Points correspond to uncensored test patients and individuals surviving beyond the last uncensored time, colored by their observed event times. In both cases, patients with similar event times cluster in contiguous regions, illustrating that the model encodes similarity in terms of process parameters.

$\{x_0, D\}$ space (Fig. 5, top row). For a given diffusion coefficient D , these patients tend to have initial conditions x_0 closer to the absorbing barrier, linking blood pressure to the only deterministic component of the underlying Brownian motion. This alignment between clinical risk factors and model-derived parameters further supports the physics-based interpretability of DeepFHT.

Final remarks. We conclude this section by noting a phenomenon visible in Figs. 4, 5: the apparent collinearity between process parameters (or their logarithms). This effect, observed in both Lévy and inverse Gaussian models, leads to data points concentrating along one-dimensional manifolds in parameter space. As reported in the FHT literature [12], this behavior can be attributed to the limited complexity of publicly available datasets rather than to intrinsic shortcomings of the models themselves. We reinforce this notion by showing that the parameter space of the synthetic NonPH dataset does not exhibit this effect (see Appendix B, Fig. 6).

VI. DISCUSSION

We introduced DeepFHT, a neural survival model that combines the flexibility of deep learning with the physics-based interpretability of first-passage-time distributions. In this work, we focused on diffusion models, for which closed-form survival functions can be derived and whose parameters admit a clear physical interpretation. Importantly, the mapping from input variables to process parameters can be implemented with *arbitrarily complex neural networks*, conferring high modeling flexibility and

strong fitting power while *maintaining physics-based interpretability* through the underlying diffusion parameters.

A central advantage of DeepFHT lies in its physics-based interpretability. By mapping individuals to points in parameter space, the model allows us to understand survival in terms of well-characterized process parameters such as initial position, drift, and diffusion. This representation provides intuitive visualizations of survival dynamics and encodes similarity between patient outcomes through distance in parameter space. In this space, DeepFHT reveals clustering of patients by event times and recovers known associations between clinical features and disease outcomes. Such interpretability sidesteps the classical issue of explainability in deep survival models and can be especially valuable in clinical settings where transparency is essential.

Finally, across multiple clinical datasets, DeepFHT achieved predictive performance comparable to or exceeding Cox regression, with clear gains in proof-of-concept scenarios characterized by nonlinear effects and violations of the proportional hazards assumption. Overall, the similar performance of the two approaches suggests limited expressiveness intrinsic to the available datasets. We expect that testing on richer datasets will highlight the value of incorporating deep learning techniques and stochastic models into modern survival analysis.

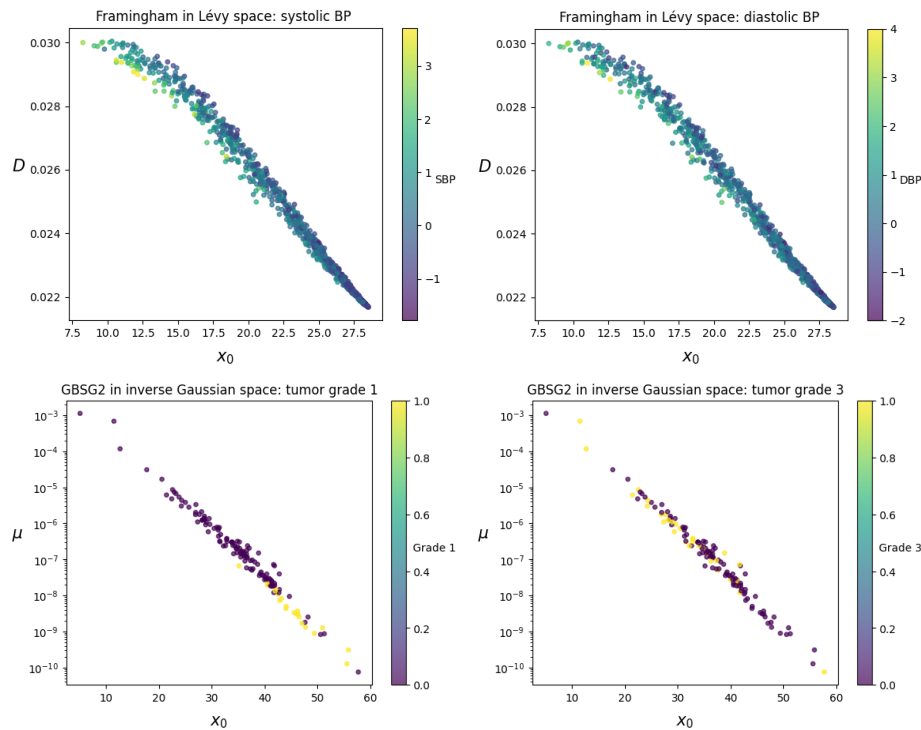


FIG. 5: Feature–parameter relationships in the Lévy and inverse Gaussian DeepFHT models. Top: Framingham dataset with Lévy model, showing the parameter space $\{x_0, D\}$ colored by systolic (left) and diastolic (right) blood pressure. Bottom: GBSG2 dataset with inverse Gaussian model, showing the parameter space $\{x_0, \mu\}$ for patients with grade 1 (left) and grade 3 (right) tumors.

In both cases, clinical risk factors align with model-derived high-risk regions (small x_0 , large D or μ), supporting the physical interpretability of the parameterization.

-
- [1] D. R. Cox, Regression models and life-tables, *Journal of the Royal Statistical Society: Series B (Methodological)* **34**, 187 (1972).
- [2] R. Tibshirani, The lasso method for variable selection in the cox model, *Statistics in Medicine* **16**, 385 (1997).
- [3] G. Ridgeway, The state of boosting, *Computing Science and Statistics* **31**, 172 (1999).
- [4] D. Faraggi and R. Simon, A neural network model for survival data, *Statistics in Medicine* **14**, 73 (1995).
- [5] O. O. Aalen, A linear regression model for the analysis of life times, *Statistics in Medicine* **8**, 907 (1989).
- [6] M. C. Pike, A method of analysis of a certain class of experiments in carcinogenesis, *Biometrics* **22**, 142 (1966).
- [7] J. H. Friedman, Greedy function approximation: A gradient boosting machine, *Annals of Statistics* **29**, 1189 (2001).
- [8] H. Ishwaran, U. B. Kogalur, E. H. Blackstone, and M. S. Lauer, Random survival forests, *Annals of Applied Statistics* **2**, 841 (2008).
- [9] J. L. Katzman, U. Shaham, A. Cloninger, J. Bates, T. Jiang, and Y. Kluger, DeepSurv: Personalized treatment recommender system using a cox proportional hazards deep neural network, *BMC Medical Research Methodology* **18**, 24 (2018).
- [10] P. Liu, B. Fu, and S. X. Yang, Hitboost: Survival analysis via a multi-output gradient boosting decision tree method, *IEEE Access* **7**, 56785 (2019).
- [11] C. Lee, W. R. Zame, J. Yoon, and M. van der Schaar, Deephit: A deep learning approach to survival analysis with competing risks, in *Proceedings of the AAAI Conference on Artificial Intelligence*, Vol. 32 (2018).
- [12] M. T. Lee and G. A. Whitmore, Threshold regression for survival analysis: Modeling event times by a stochastic process reaching a boundary, *Statistical Science* **21**, 501 (2006).
- [13] R. D. Bin and V. G. Stikbakke, A boosting first-hitting-time model for survival analysis in high-dimensional settings, *Lifetime Data Analysis* **29**, 420 (2023).
- [14] J. A. Race and M. L. Pennell, Semi-parametric survival analysis via dirichlet process mixtures of the first hitting time model, *Lifetime Data Analysis* **27**, 92 (2021).
- [15] C. W. Gardiner, *Stochastic Methods: A Handbook for the Natural and Social Sciences*, 4th ed., Springer Series in Synergetics, Vol. 13 (Springer, Berlin; Heidelberg, 2009).
- [16] O. O. Aalen, Ørnulf Borgan, and H. K. Gjessing, *Survival and Event History Analysis: A Process Point of View*, *Statistics for Biology and Health*, Vol. 46 (Springer, New York, 2008).
- [17] G. W. Brier, Verification of forecasts expressed in terms of probability, *Monthly Weather Review* **78**, 1 (1950).
- [18] E. Graf, C. Schmoor, W. Sauerbrei, and M. Schumacher, Assessment and comparison of prognostic classification

- schemes for survival data, *Statistics in Medicine* **18**, 2529 (1999).
- [19] T. Akiba, S. Sano, T. Yanase, T. Ohta, and M. Koyama, Optuna: A next-generation hyperparameter optimization framework, in *Proceedings of the 25th ACM SIGKDD International Conference on Knowledge Discovery & Data Mining (KDD '19)* (ACM, Anchorage, AK, USA, 2019) pp. 2623–2631.
 - [20] L. Antolini, P. Boracchi, and E. Biganzoli, A time-dependent discrimination index for survival data, *Statistics in Medicine* **24**, 3927 (2005).
 - [21] F. E. Harrell, R. M. Califf, D. B. Pryor, K. L. Lee, and R. A. Rosati, Evaluating the yield of medical tests, *JAMA* **247**, 2543 (1982).
 - [22] J. M. Robins and D. M. Finkelstein, Correcting for non-compliance and dependent censoring in an aids clinical trial with inverse probability of censoring weighted (ipcw) log-rank tests, *Biometrics* **56**, 779 (2000).
 - [23] E. Drysdale, Survset: An open-source time-to-event dataset repository, arXiv preprint arXiv:2203.03094 (2022).
 - [24] M. Schumacher, C. Schmidtgen, and W. Sauerbrei, The prognostic impact of age and other factors on the hazard of relapse in breast cancer, *Journal of Clinical Epidemiology* **47**, 1025 (1994).
 - [25] T. R. Dawber, G. F. Meadors, and F. E. Moore, Epidemiological approaches to heart disease: The framingham study, *American Journal of Public Health and the Nation's Health* **41**, 279 (1951).
 - [26] W. A. Knaus, F. E. Harrell, J. Lynn, L. Goldman, R. S. Phillips, A. F. Connors, N. V. Dawson, W. J. Fulkerson, R. M. Califf, and N. Desbiens, The support prognostic model: Objective estimates of survival for seriously ill hospitalized adults, *Annals of Internal Medicine* **122**, 191 (1995).
 - [27] A. Dispenzieri, J. A. Katzmann, R. A. Kyle, D. R. Larson, T. M. Therneau, L. J. Melton, S. K. Kumar, and S. V. Rajkumar, Use of nonclonal serum immunoglobulin free light chains to predict overall survival in the general population, *Mayo Clinic Proceedings* **87**, 512 (2012).
 - [28] I. Rossi, F. Sartori, C. Rollo, G. Birolo, P. Fariselli, and T. Sanavia, Beyond cox models: Assessing the performance of machine-learning methods in non-proportional hazards and non-linear survival analysis, arXiv preprint arXiv:2504.17568 (2025), 24 Apr 2025.

Appendix A: Model architecture and hyperparameters

Hyperparameter configurations Table I presents the best hyperparameter configurations obtained via cross-validation, for each dataset and distribution. For all configurations, batch normalization is applied after each hidden layer for improved training stability. Dropout is subsequently applied, if selected during cross-validation, before the activation function.

The tuned hyperparameters are:

- **Hidden sizes:** Model architecture, as a tuple indicating for each hidden layer.
- **Epochs:** Number of training epochs.
- **BS:** Batch size, computed as 2^n , where n is the original tuned exponent.
- **LR:** Learning rate.
- **DO:** Dropout probability.
- **Activation:** Activation function used in hidden layers.

TABLE I: Best hyperparameters per dataset and distribution. Batch normalization is always applied after each hidden layer.

Dataset	Model	Hidden Sizes	Activation	DO	Epochs	BS	LR
GBSG2	Levy	16	tanh	0.2	150	64	0.0012
	InverseGaussian	16,16	elu	0.5	350	32	0.0005
Framingham	Levy	16,16	tanh	0.5	150	64	0.0011
	InverseGaussian	16,16	elu	0.2	300	32	0.0003
SUPPORT2	Levy	32,16	elu	0.3	300	32	0.0003
	InverseGaussian	32,16	relu	0.4	200	32	0.0001
FLChain	Levy	16,16	tanh	0.1	450	32	0.0006
	InverseGaussian	16	elu	0.5	450	256	0.0030
NonPH	Levy	16,16	relu	0.0	450	256	0.0039
	InverseGaussian	16,16	relu	0.0	200	64	0.0028

Cross validation scores In Table II we present validation C-index scores of our model across datasets and distributions. For each pair, we report the mean score across cross-validation folds and the corresponding standard deviation.

Model	GBSG2	Framingham	SUPPORT2	FLChain	NonPH
Lévy	0.694 ± 0.017	0.705 ± 0.012	0.854 ± 0.004	0.929 ± 0.003	0.840 ± 0.004
Inverse Gaussian	0.692 ± 0.024	0.700 ± 0.013	0.854 ± 0.005	0.926 ± 0.003	0.837 ± 0.010

TABLE II: Cross-validation C-indices for Lévy and inverse Gaussian models across datasets.

Appendix B: NonPH parameter space

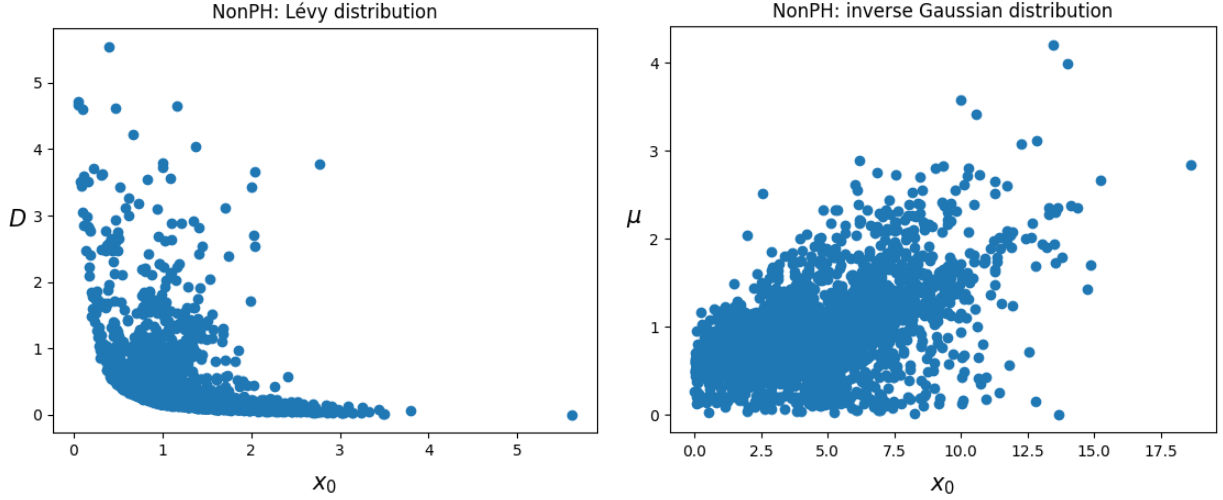


FIG. 6: NonPH test set in the parameter spaces of Lévy and inverse Gaussian DeepFHT models. Notice the absence of collinearity between parameters, as discussed in Sec. VB

Appendix C: Synthetic dataset generation

The synthetic dataset NonPH was constructed to strongly violate Cox Regression assumptions, namely proportional hazards and linearity. Here we describe in detail the procedure used to generate it.

First, we built a matrix of 10,000 observations, each with 20 features x_1, \dots, x_{20} randomly sampled from a normal distribution. Event times were randomly sampled within the interval $[0, 10]$, which was discretized into 1,000 equally sized sub-intervals, plus an additional unbounded $[10, +\infty[$ interval. For each observation, we defined a discrete probability distribution over these intervals as the probability that an event occurs in them according to a specific survival function parametrized by the features. A single interval was then sampled, with its lower bound taken as the event time for bounded intervals or as the censoring time for the unbounded interval. This ensured that all events occurred before time 10 and all censoring at time 10. To enforce consistency, additional censoring was applied so that 25% of observations were censored. Finally, a random subset of 2,400 observations was retained, preserving the censoring ratio, both to reduce computational cost and to reflect a more realistic dataset size.

The survival distribution used for the event sampling was defined as follows. The time interval $[0, 10]$ was partitioned into 16 intervals of equal length where the distribution density is a constant on each interval with value p_i for $i = 1, \dots, 16$. The p_i were computed using the soft-max function on the first 16 features (one for each time interval) multiplied by 16:
$$p_i = \frac{\exp(16x_i)}{\sum_{j=1}^{16} \exp(16x_j)}.$$

The softmax function can be interpreted as a smooth approximation of the argmax operator. When all inputs are scaled by a coefficient β , the approximation becomes improves: as β increases, the probability p_i associated with the largest input x_i approaches 1, while the others tend toward 0. We set $\beta = 16$ (coincidentally matching the number of intervals) so that, for most individuals, the event probability is concentrated in a single time interval. With a smaller value such as $\beta = 1$, the resulting distributions would be flatter and therefore easier to approximate for PH assuming methods.